Osteochondral Lesions of the Knee: Differentiating the Most Common Entities at MRI

Tetyana Gorbachova, MD
Yulia Melenevsky, MD
Micah Cohen, MD
Brett W. Cerniglia, MD

Abbreviations: AVN = avascular necrosis, OCD = osteochondritis dissecans, SIF = subchondral insufficiency fracture

RadioGraphics 2018; 38:1478–1495

https://doi.org/10.1148/rg.2018180044

Content Codes: ER MK MR PD

From the Department of Radiology, Einstein Healthcare Network, 5501 Old York Rd, Philadelphia, PA 19141 (T.G, M.C., B.W.C.) and Department of Radiology, University of Alabama at Birmingham, Birmingham, Ala (Y.M.). Recipient of a Magna Cum Laude award for an education exhibit at the 2017 RSNA Annual Meeting. Received March 1, 2018; revision requested April 5 and received April 26; accepted May 4. For this journal-based SA-CME activity, the authors, editor, and reviewers have disclosed no relevant relationships. **Address correspondence to** T.G. (e-mail: *gorbacht@einstein.edu*).

SA-CME LEARNING OBJECTIVES

After completing this journal-based SA-CME activity, participants will be able to:

- Describe the anatomy of the osteochondral junction with MRI correlation.
- Contrast and compare common entities that manifest as osteochondral lesions of the knee: acute traumatic osteochondral injuries, AVN, SIF of the knee, OCD, bone marrow edema-like lesions, and subchondral cystlike lesions in osteoarthritis.
- Evaluate MRI findings of each condition and how they pertain to treatment.

See rsna.org/learning-center-rg.

An earlier incorrect version of this article appeared online. This article was corrected on August 23, 2018.

Several pathologic conditions may manifest as an osteochondral lesion of the knee that consists of a localized abnormality involving subchondral marrow, subchondral bone, and articular cartilage. Although understanding of these conditions has evolved substantially with the use of high-spatial-resolution MRI and histologic correlation, it is impeded by inconsistent terminology and ambiguous abbreviations. Common entities include acute traumatic osteochondral injuries, subchondral insufficiency fracture, so-called spontaneous osteonecrosis of the knee, avascular necrosis, osteochondritis dissecans, and localized osteochondral abnormalities in osteoarthritis. Patient demographics, the clinical presentation, and the role of trauma are critical for differential diagnosis. A localized osteochondral defect can be created acutely or can develop as an end result of several chronic conditions. MRI features that aid in diagnosis include the location and extent of bone marrow edema, the presence of a fracture line, a hypointense area immediately subjacent to the subchondral bone plate, and deformity of the subchondral bone plate. These findings are essential in diagnosis of acute traumatic injuries, subchondral insufficiency fracture, and its potentially irreversible form, spontaneous osteonecrosis of the knee. If the lesion consists of a subchondral region demarcated from the surrounding bone, the demarcation should be examined for completeness and the presence of a "double-line sign" that is seen in avascular necrosis or findings of instability, which are important for proper evaluation of osteochondritis dissecans. Subchondral bone plate collapse, demonstrated by the presence of a depression or a fluid-filled cleft, can be seen in advanced stages of both avascular necrosis and subchondral insufficiency fracture, indicating irreversibility. Once the diagnosis is established, it is important to report pertinent MRI findings that may guide treatment of each condition.

Introduction

Several pathologic conditions may manifest as an osteochondral lesion of the knee, which is a localized abnormality of the subchondral marrow, subchondral bone, and articular cartilage. There is an overlap in patterns of signal intensity alterations and morphologic abnormalities among these conditions at MRI, while the clinical significance of each lesion and the treatment implications are different. Understanding of these conditions evolved with clinical use of high-spatial-resolution MRI combined with the availability of histologic correlation. This article provides a comparative analysis of several of the most common entities that manifest as osteochondral lesions of the knee, in particular of the femoral condyles. We offer a summary of current concepts for each condition to aid in their differentiation at MRI. Typical patient demo-

TEACHING POINTS

- An osteochondral defect can occur acutely or develop as a result of several chronic conditions including *(a)* separation of the osteochondral fragment caused by an acute traumatic injury or as the end result of an unstable fragment in osteochondritis dissecans (OCD), *(b)* acute osteochondral impaction of the bone with resultant contour deformity, and *(c)* a collapse of the subchondral bone in a subchondral insufficiency fracture (SIF) or avascular necrosis (AVN) or a bone collapse uncovering a large subchondral cyst.
- A subchondral fracture appears as a subchondral linear hypointensity, without an associated contour deformity or visible involvement of the articular surface. Osteochondral fractures involve both articular cartilage and the subchondral bone plate and appear as a fracture line that violates the joint surface, subchondral bone plate depression, articular surface disruption and fragmentation, or a combination of these features.
- The findings in SIF include *(a)* a hypointense line that is irregular, sometimes discontinuous, or open-ended in the subarticular marrow at a variable distance from the epiphyseal surface and curvilinear or parallel to the subchondral bone plate, which is the subchondral fracture callus and granulation tissue; *(b)* an area of low signal intensity immediately subjacent to and creating the appearance of a thickened subchondral bone plate, which is a combination of fracture with callus and granulation tissue and secondary osteonecrosis between the fracture line and the articular surface; *(c)* a deformity of the subchondral bone plate defined as either subtle flattening or a focal depression that represents a subchondral bone plate fracture, and *(d)* a fluid-filled cleft underlying the subchondral bone plate, indicating its gross collapse and separation.
- Early AVN of the femoral condyle appears as an area of necrotic marrow that contains fatty marrow (or red marrow in patients <1 year old) outlined by a distinct rim of sclerosis. This rim, typically hypointense at MRI, is a reactive interface between necrotic and viable bone, often reaching the subchondral bone plate. In some cases, it completely circumscribes centrally located epiphyseal marrow. In most cases, a "double-line sign," an inner high-signal-intensity band (vascularized granulation tissue, or the "creeping zone of substitution") and an outer low-signal-intensity band (sclerotic appositional new bone), are visible on T2-weighted and intermediate-weighted MR images. The interface represents live tissue reaction, and, unlike a fracture line, it is complete and encircles the infarcted area without interruption.
- Two essential factors allow determination of the prognosis and treatment strategies for OCD: the skeletal maturity of the patient and the stability of the lesion. Skeletal maturity must be determined first, because MRI criteria for instability for adults differ from those for juvenile OCD.

graphics and clinical presentation, the etiologic role of trauma, and classic MRI features that help to guide appropriate treatment are described for each entity (Table).

Terminology

Several descriptive terms and abbreviations can be applied to focal abnormalities of the articular cartilage and subchondral bone.

Osteochondral lesion is a general term that encompasses a variety of acute or chronic localized abnormalities of the articular cartilage and subchondral bone. Although it is adopted for osteochondral abnormalities of the talus (1), the term lacks specificity and should be only part of a description of a more specific diagnostic entity.

Osteochondral defect is a term for a localized defect of the articular cartilage and subchondral bone. It is a morphologic finding that may be seen in various conditions and that produces a scalloped defect along the articular surface of the bone (Fig 1). An osteochondral defect can occur acutely or develop as a result of several chronic conditions including *(a)* separation of the osteochondral fragment caused by an acute traumatic injury or as the end result of an unstable fragment in osteochondritis dissecans (OCD), *(b)* acute osteochondral impaction of the bone with resultant contour deformity, and *(c)* a collapse of the subchondral bone in a subchondral insufficiency fracture (SIF) or avascular necrosis (AVN) or a bone collapse uncovering a large subchondral cyst. In clinical practice, the abbreviation OCD is often used for both osteochondral defect and osteochondritis dissecans, which causes confusion. For the purposes of this article, the abbreviation OCD will be used only for osteochondritis dissecans.

Osteochondritis dissecans (OCD) is a term for a distinct clinical-pathologic entity: a pathologic condition that affects subchondral bone formation and may result in an unstable subchondral fragment, disruption of adjacent articular cartilage, and possible separation of the fragment. The actual defect may or may not be present on MR images, depending on the stage of the process.

Anatomy and MRI Appearance of the Osteochondral Junction

When evaluating an osteochondral lesion, a radiologist must consider several anatomic and technical aspects to accurately assess the articular cartilage, the subchondral bone plate, and the underlying subchondral bone marrow. Histologically, articular cartilage is organized into four layers, each characterized by a different cellular composition and orientation of collagen fibers that produce gradual variations in signal intensity: superficial, transitional, deep (radial), and calcified layers (2). The MRI appearance of individual layers depends on both anatomic and technical factors. The highly organized collagen network in the cartilage displays T2 anisotropy, and the regional variations in cartilage signal intensity are affected by the "magic angle" effect (3) (Fig 2). The deepest calcified cartilage layer is located at the interface with the subchondral bone plate, a layer of compact cortical bone that overlies the cancellous marrow-containing trabecular bone. The compact subchondral

Summary of Clinical and MRI Features of Common Osteochondral Lesions of the Knee

Differentiating Features	Acute Osteochondral Fracture	SIF and So-called SONK	AVN (Primary Osteonecrosis)	OCD	Osteoarthritis*
Patient age	Any age Young active patients	Older patients	Adults, typically aged 40–60 years	Childhood to middle age; most frequent onset in preadolescence	Adults, elderly patients
Risk factors	...	Bone weakening (eg, osteoporosis)	Use of corticosteroid therapy Alcoholism	Incompletely healed juvenile OCD may become adult OCD	...
Location	Depends on the mechanism of injury	MFC (90%), LFC, tibial plateaus Classic: weight-bearing surface of the MFC	Ischemic necrosis of bone: any location Collapse: weight-bearing surface	Most often in MFC then in LFC and then in the patella Classic: lateral (intercondylar) aspect of MFC (51%)	Most commonly weight-bearing surface May involve any area
Role of trauma	Acute trauma	Minimal or no trauma	No trauma	Chronic repetitive stress in active children, particularly high-level athletes	None in primary osteoarthritis
Mechanism	Abnormal force applied to normal trabeculae Osteochondral injury is typically produced by an internal force	Physiologic force applied to weakened trabeculae (and diminished protective function of articular cartilage and/or menisci) leading to a SIF; may progress to secondary localized osteonecrosis, articular surface collapse, and progressive osteoarthritis	Causes of collapse: Fatigue microfractures in the necrotic zone Osteoclastic activity in the reparative front Focal concentration of stress at the AVN margins	Hypothesis: disturbance of secondary ossification center leading to localized delay in subchondral bone formation, and subsequent failure of overlying cartilage, localized articular surface fragmentation and separation	Synovial fluid intrusion theory Bone contusion theory
Clinical presentation	Acute onset of pain	Sudden onset, severe and unrelenting knee pain	Vague pain, greatly exacerbated at the onset of collapse	Poorly localized knee pain for >1 year, often exacerbated by exercise Acute mechanical symptoms with dislodgement of fragment	Chronic pain
MRI findings pertinent to management	Soft-tissue injuries associated with characteristic osseous injury patterns	Features associated with risk of irreversibility and poor prognosis† Meniscal abnormality, particularly radial and root tears	Size and location of AVN Features of articular collapse	Skeletal maturity Fragment: size, location, features of instability, integrity, and composition (mineralized or not)†	Extent of cartilage loss Presence of BMLs Meniscal abnormality

Note.—AVN = avascular necrosis, BML = bone marrow edema-like lesion, LFC = lateral femoral condyle, MFC = medial femoral condyle, OCD = osteochondritis dissecans, SIF = subchondral insufficiency fracture, SONK = spontaneous osteonecrosis of the knee.
*With subchondral cystlike lesions.
†See text for description of specific features.

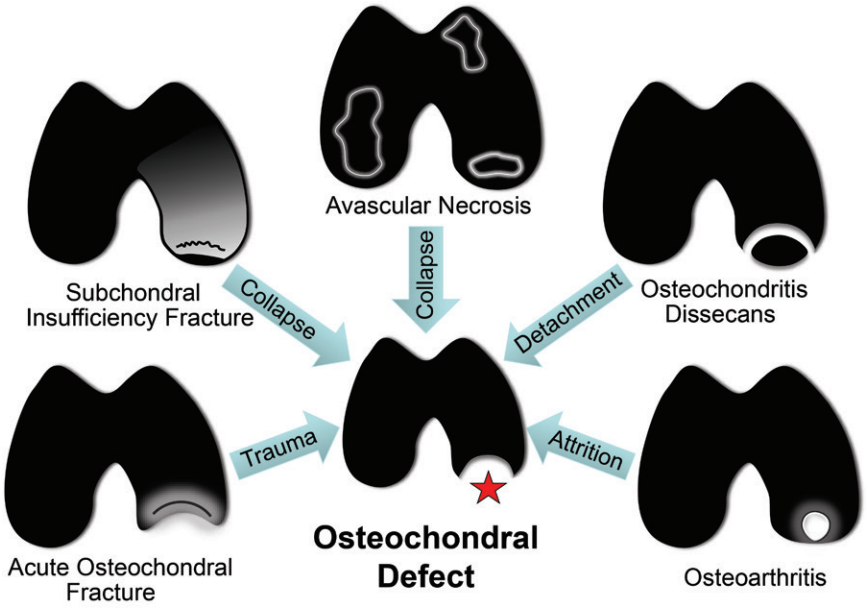

Figure 1. Osteochondral defect. An osteochondral defect of the femoral condyle (☆) may be the result of several acute and chronic conditions that produce a surface deformity with a localized defect of the articular cartilage and subchondral bone.

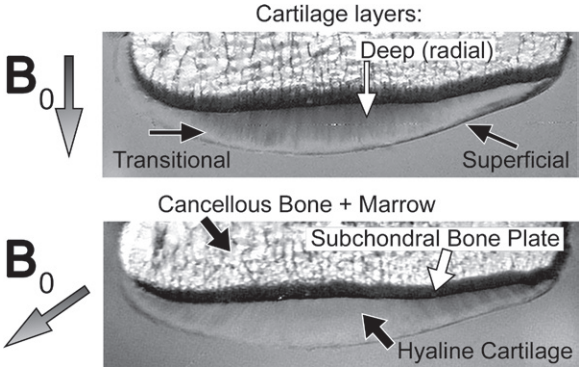

Figure 2. MRI appearance of the osteochondral junction. In vitro T2-weighted spin-echo MR images of the tibial plateau at 7 T in the same specimen oriented perpendicularly to the main magnetic field (B_0, gray arrow, top image) and tilted 55° to B_0 (bottom image) show the typical layered appearance of the articular cartilage. The regional variations in cartilage signal intensity are affected by the magic angle. Changes in the orientation relative to B_0 alter the appearance of the cartilage. The thickness of the subchondral bone plate on these images is exaggerated by the chemical shift of the marrow fat signal. (MR images courtesy of Douglas W. Goodwin, MD, Dartmouth Geisel School of Medicine.)

bone and calcified cartilage are collectively termed the *subchondral plate* (4,5). The calcified cartilage layer may be unmasked by using very short echo time (often referred to as "ultrashort" echo time) imaging (2,6); however, it cannot be separated from the subchondral bone during routine clinical pulse sequences. The two layers appear as one low-signal-intensity band overlying the subarticular marrow. We refer to this band as the *subchondral bone plate*.

The apparent thickness of the subchondral bone plate also may be altered by chemical shift misregistration artifact caused by the high–fat-content voxels of the underlying bone marrow, which results in a substantially thicker appearance of the subchondral bone plate (7,8).

Acute Traumatic Osteochondral Injury

The spectrum of acute traumatic injuries to the articular surface of the bone includes bone bruises and chondral, subchondral, and osteochondral fractures. The terms *bone bruise* or *bone contusion* refer to trabecular microfractures that manifest as a pattern of bone marrow edema on MR images, without contour abnormalities or a discrete fracture line (2,9,10). Such edema appears speckled and poorly defined.

In the acute setting, the fracture line is best shown on T1-weighted MR images as a linear hypointensity. It may be less conspicuous on T2-weighted images when it is hyperintense and surrounded by bone marrow edema, unless there is a component of trabecular impaction that renders the fracture hypointense on both T1- and T2-weighted MR images, similar to the appearance of stress fractures. A subchondral fracture appears as a subchondral linear hypointensity, without an associated contour deformity or visible involvement of the articular surface (Fig 3). Osteochondral fractures involve both articular cartilage and the subchondral bone plate and appear as a fracture line that violates the

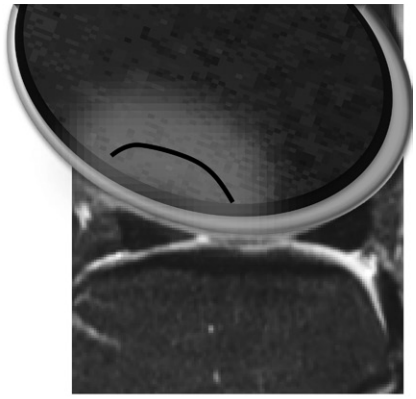

a.

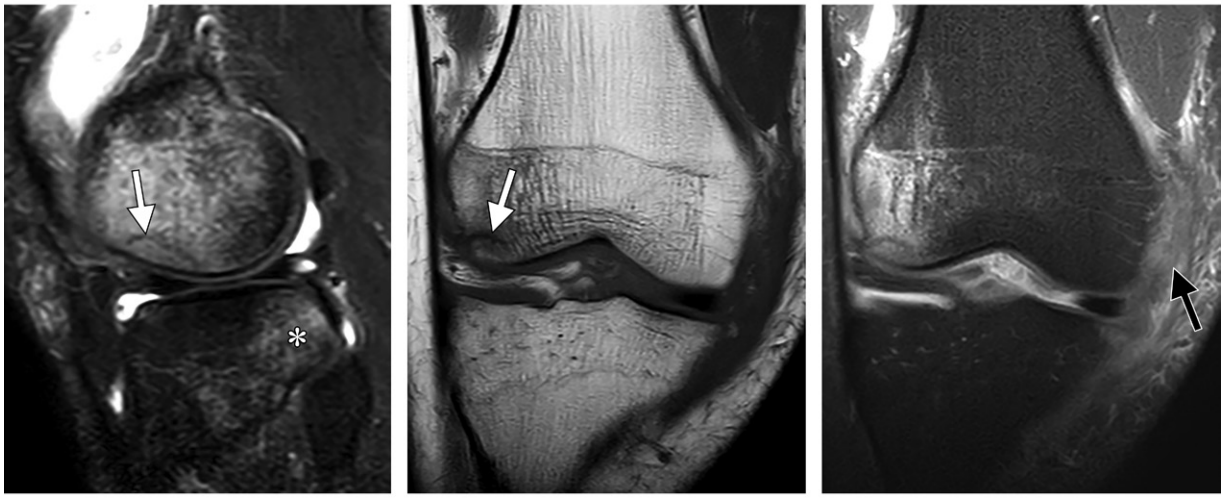

b. c. d.

Figure 3. Subchondral fracture in a 32-year-old man with an acute medial collateral ligament tear (arrow in **d**) and an anterior cruciate ligament rupture (not shown). Diagram of the fluid-sensitive MR image **(a)** and sagittal T2-weighted fat-suppressed **(b)**, coronal T1-weighted **(c)**, and proton-density–weighted fat-suppressed **(d)** MR images show a subchondral fracture (arrow in **b** and **c**) as a curvilinear hypointensity surrounded by bone marrow edema, without associated contour deformity. A bone contusion (∗ in **b**) at the lateral tibial plateau can be distinguished from a fracture because of the absence of a contour deformity or fracture line.

joint surface, subchondral bone plate depression, articular surface disruption and fragmentation, or a combination of these features (Fig 4) (9,10). A curvilinear fracture may completely encircle a portion of the subchondral bone and the overlying cartilage, creating an osteochondral fragment (Fig 5).

In general, these injuries are more common in young active patients and usually are the result of high-impact force applied to a normal bone that has sustained an acute injury. Such force is typically internal, related to the contact of one bone with a neighboring bone during the traumatic event (9). Patients present with acute onset of pain and have a clear history of preceding trauma. Osteochondral injury is commonly associated with immediate effusion that represents hemarthrosis or lipohemarthrosis. The location of the abnormality is dictated by the mechanism of injury. Several typical patterns of osteochondral injuries have been described in association with certain types of internal derangement and instability (11–13). Once a characteristic pattern of osseous injury is recognized on MR images, the radiologist must seek specific additional soft-tissue and osseous injuries.

SIF and Spontaneous Osteonecrosis of the Knee

A peculiar clinical-radiologic entity originally designated as a so-called spontaneous osteonecrosis of the knee (SONK, a misnomer) was recognized early as a distinct form of epiphyseal osteonecrosis (14). This condition typically is seen in older patients after the 6th decade of life and more frequently in women. Patients often report a sudden onset of severe and unrelenting knee joint pain related to minimal or no trauma and often recall a precise moment when the symptoms started.

Two misconceptions contributed to a long evolution of the understanding of this disorder: *(a)* a pre–MRI-era hypothesis that attributed it to a primary AVN, resulting in the misnomer, and *(b)* an effort to distinguish it fundamentally from SIF, largely impelled by differences in prognosis. A study by Yamamoto and Bullough (15), which was supported by results of a later study (16), showed that the primary event is a SIF, followed by secondary necrosis limited to the area between the fracture line and the subchondral bone plate. MRI features of this lesion also have been shown to be profoundly different from those of primary AVN (17,18). SIF

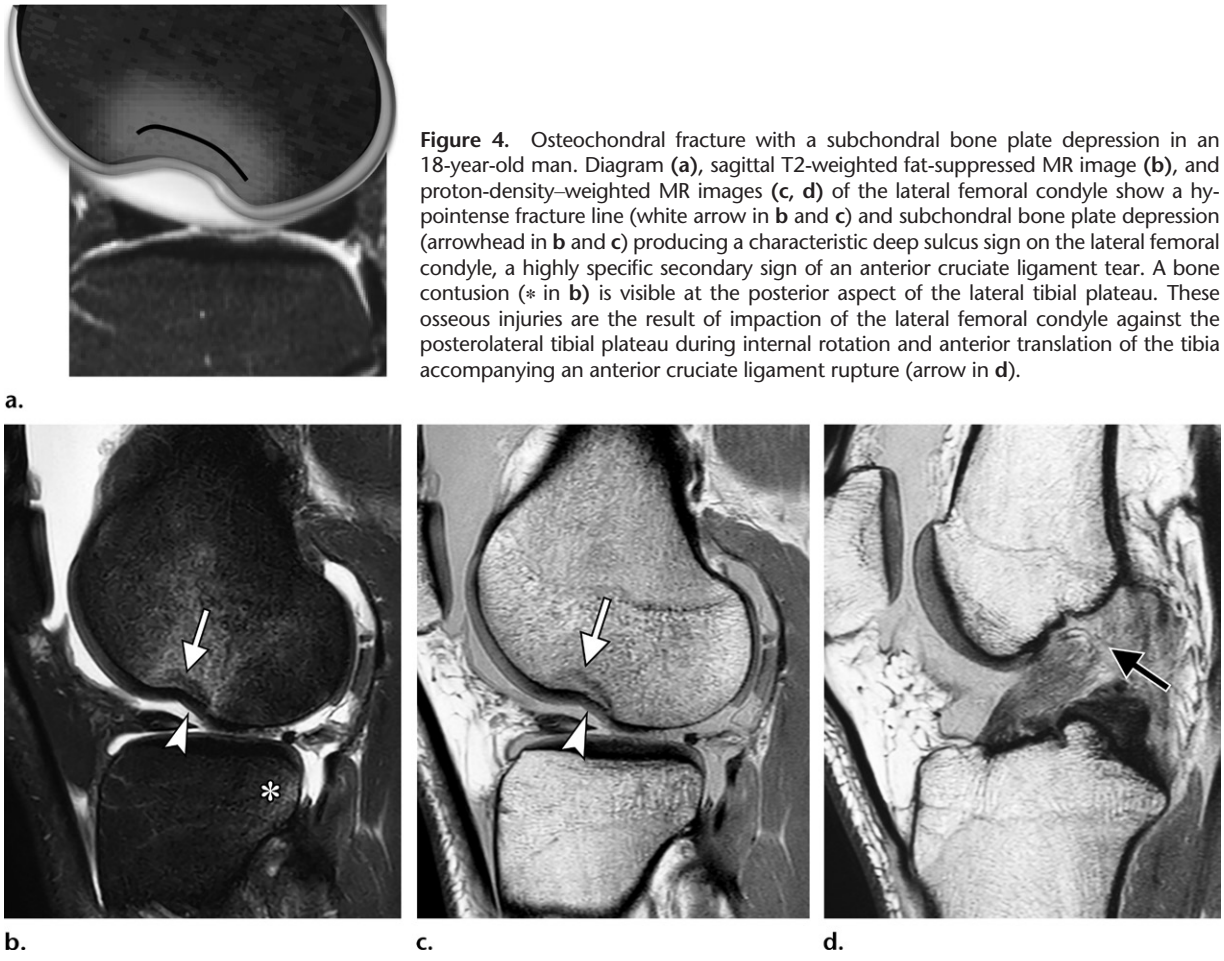

Figure 4. Osteochondral fracture with a subchondral bone plate depression in an 18-year-old man. Diagram **(a)**, sagittal T2-weighted fat-suppressed MR image **(b)**, and proton-density–weighted MR images **(c, d)** of the lateral femoral condyle show a hypointense fracture line (white arrow in **b** and **c**) and subchondral bone plate depression (arrowhead in **b** and **c**) producing a characteristic deep sulcus sign on the lateral femoral condyle, a highly specific secondary sign of an anterior cruciate ligament tear. A bone contusion (∗ in **b**) is visible at the posterior aspect of the lateral tibial plateau. These osseous injuries are the result of impaction of the lateral femoral condyle against the posterolateral tibial plateau during internal rotation and anterior translation of the tibia accompanying an anterior cruciate ligament rupture (arrow in **d**).

a.

b. **c.** **d.**

involves a physiologic force applied to weakened trabeculae, often in association with osteopenia and diminished protective function of the articular cartilage and meniscus, which leads to a fracture along the subchondral area of the bone. Such a fracture can either stabilize or progress to a frank collapse of the articular surface that is associated with pain and progressive osteoarthritis and eventually necessitates knee replacement.

Because of the proven microtraumatic origin of SONK and the histopathologic and MRI features that unite it with SIF, it is currently accepted that a SONK is a SIF that has progressed into collapse, with secondary necrosis found in the collapsed specimens. When evaluating SIF, radiologists must report established MRI features associated with such poor outcomes (17).

SIFs typically are observed along the central weight-bearing aspect of the femoral condyle (60%–90%), but they also may involve the central tibial plateau, and less commonly, the periphery of the articular surface (18–21). At MRI, SIF is associated with marked bone marrow edema emanating from the subchondral region and extending over large areas (10,17,18), often involving the entire femoral condyle. This differs from the more localized bone marrow edema lesion subjacent to cartilage loss in osteoarthritis (10). However, the extent of bone marrow edema has no prognostic significance (17,21).

More important are the localized abnormalities in the subchondral region, best shown on T2-weighted and proton-density–weighted MR images. The findings in SIF include *(a)* a hypointense line that is irregular, sometimes discontinuous, or open-ended in the subarticular marrow at a variable distance from the epiphyseal surface and curvilinear or parallel to the subchondral bone plate (Fig 6), which is the subchondral fracture callus and granulation tissue (15); *(b)* an area of low signal intensity immediately subjacent to and creating the appearance of a thickened subchondral bone plate (Fig 7), which is a combination of fracture with callus and granulation tissue and secondary osteonecrosis between the fracture line and the articular surface (15,16,22); *(c)* a deformity of the subchondral bone plate defined as either subtle flattening or a focal depression that represents a subchondral bone plate fracture (Figs 8, 9); and *(d)* a fluid-filled cleft underlying the subchondral bone plate, indicating its gross collapse and separation (19) (Fig 9).

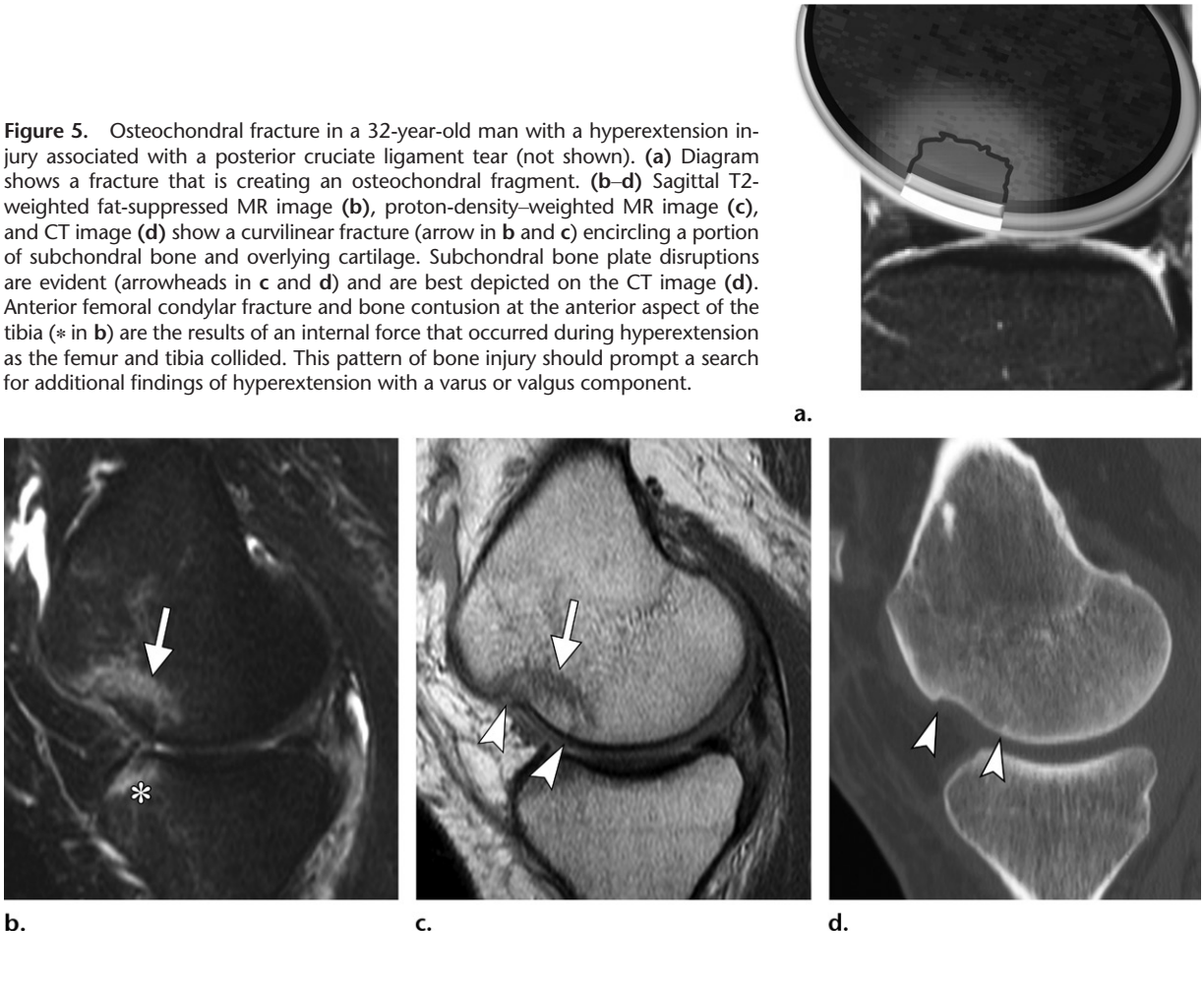

Figure 5. Osteochondral fracture in a 32-year-old man with a hyperextension injury associated with a posterior cruciate ligament tear (not shown). **(a)** Diagram shows a fracture that is creating an osteochondral fragment. **(b–d)** Sagittal T2-weighted fat-suppressed MR image **(b)**, proton-density–weighted MR image **(c)**, and CT image **(d)** show a curvilinear fracture (arrow in **b** and **c**) encircling a portion of subchondral bone and overlying cartilage. Subchondral bone plate disruptions are evident (arrowheads in **c** and **d**) and are best depicted on the CT image **(d)**. Anterior femoral condylar fracture and bone contusion at the anterior aspect of the tibia (∗ in **b**) are the results of an internal force that occurred during hyperextension as the femur and tibia collided. This pattern of bone injury should prompt a search for additional findings of hyperextension with a varus or valgus component.

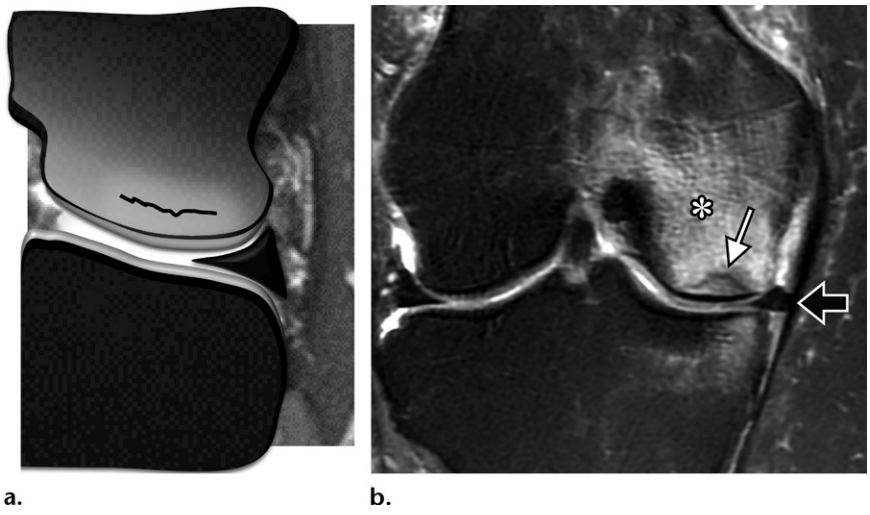

Figure 6. SIF in a 51-year-old woman with atraumatic sudden onset of knee pain and swelling. Diagram **(a)** and coronal proton-density–weighted fat-suppressed MR image **(b)** show an irregular hypointense line parallel to the subchondral bone plate **(a)** and curvilinear and open-ended laterally (white arrow in **b**), amid extensive bone marrow edema–like signal intensity in the subchondral region (∗). Note the peripheral extrusion of the medial meniscus (black arrow in **b**) from a posterior horn tear (not shown). Unlike the appearance in primary osteonecrosis, the line is incomplete, and edema appears on both sides of the line.

Among these localized abnormalities, the area of low signal intensity immediately subjacent to a subchondral bone plate is of utmost importance in early lesions; it is considered to be an essential finding observed in almost all cases of clinical SONK. If it is thicker than 4 mm or

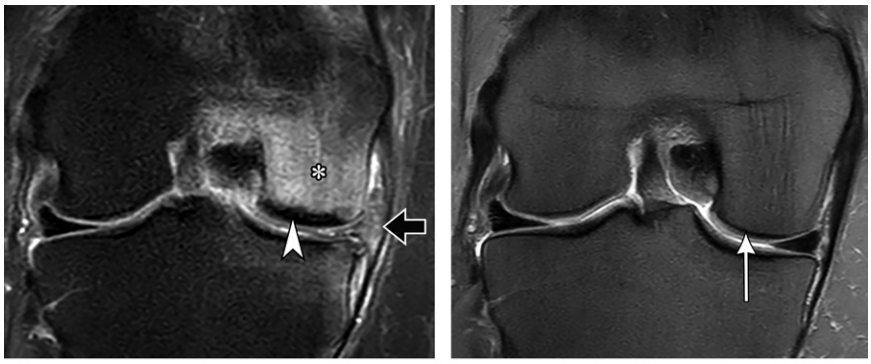

a. b.

Figure 7. SIF in a 64-year-old woman with a complex tear in the medial meniscus with peripheral extrusion (arrow in **a**). **(a)** Coronal proton-density–weighted fat-suppressed image shows an extensive bone marrow edema pattern involving the medial femoral condyle (*), accompanied by a subchondral area of low signal intensity (arrowhead) located immediately subjacent to a subchondral bone plate, producing its apparent thickening. **(b)** Coronal MR image obtained 2 years earlier shows the normal appearance of the subchondral bone plate (arrow).

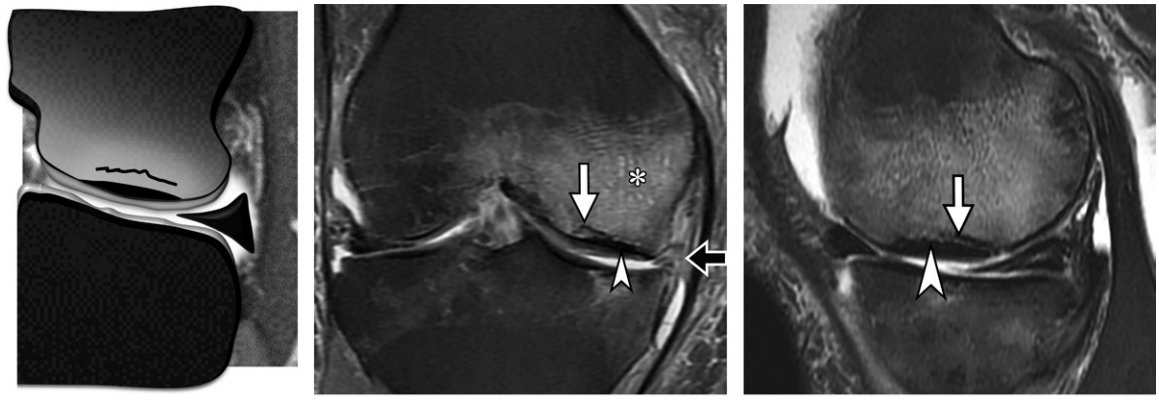

a. b. c.

Figure 8. Classic SIF in a 64-year-old man. Diagram **(a)**, coronal proton-density–weighted fat-suppressed MR image **(b)**, and sagittal T2-weighted fat-suppressed image **(c)** show a bone marrow edema pattern "painting" the entire medial femoral condyle (* in **b**). Both a subchondral hypointense line (white arrow in **b** and **c**) and a subchondral area of low signal intensity (arrowhead in **b** and **c**) are observed along the weight-bearing aspect of the condyle and are associated with subtle flattening of the articular surface. Similar findings were present on the tibial side. Note the macerated and extruded medial meniscus (black arrow in **b**).

longer than 14 mm, the lesion may be irreversible and may evolve into irreparable epiphyseal collapse and articular destruction (17). These criteria apply to lesions without an overlying cartilage abnormality (19). Subchondral hypointense fracture lines tend to resolve with conservative therapy and can be seen in patients with transient reversible SIF and in 78% of those with clinical SONK. While subtle contour deformities occasionally can be observed in self-resolving lesions, prominent contour deformity and a subchondral fluid-filled fracture cleft, both representing frank collapse of the subchondral bone plate, are poor prognostic factors (19); these features are identical to the findings of a collapse in primary AVN. A saucerized defect of the articular surface may develop in advanced cases (23,24) (Fig 10).

SIFs are associated with meniscal tears in the same compartment in 76%–94% of patients (18,20,21). More specifically, more than 50% of patients demonstrate radial and posterior root tears (20). These types of tears dramatically increase contact pressure across the joint (25). This association and a link between SIF and meniscectomy (26) support the proposed role of mechanical stress in the development of SIF and emphasize the rationale for meniscal conservation. Although they are not essential for the diagnosis of SIF, associated cartilage abnormalities are often present (18,21). The overall extent of meniscal abnormality and cartilage loss in the joint and decreased knee range of motion at the time of presentation are associated with clinical progression (21).

Initial treatment of SIF is conservative, consisting of protected weight bearing and administration

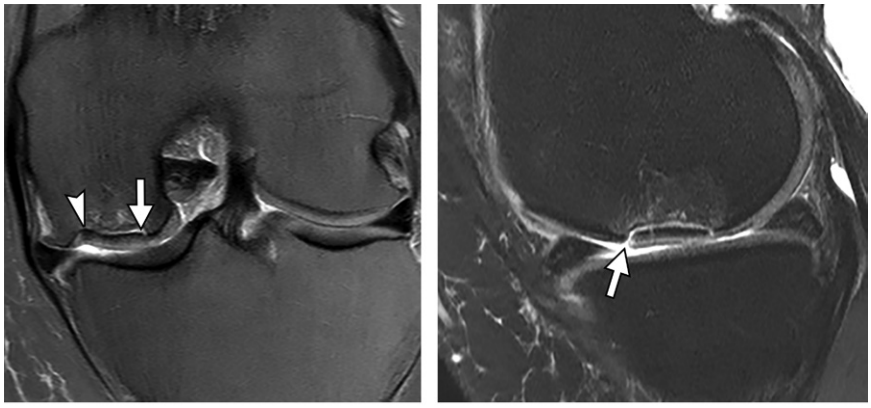

a. b.

Figure 9. Advanced SIF in a 69-year-old woman with several months of unrelenting knee pain after walking down stairs. Coronal proton-density–weighted fat-suppressed **(a)** and sagittal T2-weighted **(b)** MR images show articular surface collapse with a depression of the subchondral bone plate (arrowhead in **a**) and a fluid-filled fracture cleft underlying the subchondral bone plate (arrow). The clinical scenario and histologic findings are typical of secondary osteonecrosis. The diagnosis was a collapsed SIF with secondary osteonecrosis (SONK).

of analgesic medications to prevent development or worsening of subchondral bone collapse (27). Larger lesions with progressive articular collapse and persistent pain may require surgery (often total knee arthroplasty). Subchondroplasty, a procedure developed to treat bone marrow edema lesions by injecting a bone substitute, is one of the evolving treatment options for patients with SIF. Currently, to our knowledge, there are no data regarding which MRI features may predict improved outcomes in these patients.

AVN (Primary Osteonecrosis)

Osteonecrosis is a common condition that is the result of a reduction or complete loss of blood supply to the bone. While osteonecrosis can be idiopathic, common causes of osteonecrosis include trauma, use of corticosteroids, sickle cell anemia, collagen vascular disease, and alcoholism (28). Osteonecrosis of the knee can be encountered in epiphyseal or subarticular bone, where it is referred to as an AVN, and in the metadiaphysis, where the term *bone infarction* is often applied. Osteonecrosis tends to develop in adults, most commonly in the 4th and 5th decades of life (19). It can manifest clinically with vague pain, or there may be no symptoms until development of subchondral bone plate fracture, (ie, collapse).

The literature on osteonecrosis of femoral condyles is often mixed with and sometimes dedicated entirely to spontaneous osteonecrosis of the knee. This misnomer was entrenched in the medical lexicon for many years, persisting after recognition of this entity as a SIF (15,16). With regard to true primary osteonecrosis of the knee, general imaging principles of primary osteonecrosis can be applied, and some features established in studies of AVN of the hip can be extrapolated (19,29).

Early AVN of the femoral condyle appears as an area of necrotic marrow that contains fatty marrow (or red marrow in patients <1 year old) outlined by a distinct rim of sclerosis. This rim, typically hypointense at MRI, is a reactive interface between necrotic and viable bone, often reaching the subchondral bone plate. In some cases, it completely circumscribes centrally located epiphyseal marrow. In most cases, a "double-line sign," an inner high-signal-intensity band (vascularized granulation tissue, or the "creeping zone of substitution") and an outer low-signal-intensity band (sclerotic appositional new bone), are visible on T2-weighted and intermediate-weighted MR images (Fig 11). The interface represents live tissue reaction, and, unlike a fracture line, it is complete and encircles the infarcted area without interruption. It typically appears as undulating and convex to the articular surface; however, the shape of the line is not pathognomonic because it depends on the size and location of the infarct.

The clinical significance of AVN largely depends on the likelihood or presence of articular collapse. Several factors are responsible for development of a collapse that signifies failure of the subchondral bone plate: *(a)* the cumulative effect of fatigue microfractures in the necrotic zone, *(b)* osteoclastic activity that causes weakening of the trabeculae in the reparative front, and *(c)* focal concentration of mechanical stress on thickened bone trabeculae of the reparative zone along the AVN margins that act as "stress risers" (31–33). Collapse begins at the lateral boundary of the necrotic lesion and, depending

a.

b.

c.

Figure 10. Irreversible SIF of the lateral femoral condyle progressing to articular collapse in a 61-year-old man who presented with acute knee pain after a fall. Coronal T1-weighted, proton-density–weighted fat-suppressed, and sagittal T2-weighted fat-suppressed MR images (left to right in each row of **a**, **b**, and **c**) at presentation **(a)** show extensive bone marrow edema (* in **a**), hypointense fracture lines, and areas of low signal intensity subjacent to the subchondral bone plate (arrowheads in **a**) associated with minimal flattening of the articular surface; images obtained 6 months later **(b)** show articular surface collapse (black arrow in **b**) associated with numerous cystlike areas (white arrow in **b**) and marrow edema confined to the periarticular region; images obtained at 16 months **(c)** show that a large saucerized articular surface defect has formed (arrows in **c**).

on the size of the lesion, propagates either along the subchondral region or in the deep necrotic region (33). The risk of collapse in the femoral condyle seems to be related directly to the size and location of the infarct: Lesions involving more than one-third of the condyle on midcoronal MR images or the middle and posterior one-third of the condyle on midsagittal MR images are at higher risk of collapse (34).

It is important to recognize the MRI appearance of this critical complication of AVN that leads to premature osteoarthritis. In early uncomplicated AVN, the marrow signal in the infarct is preserved, representing mummified fat, and there is no surrounding bone marrow edema. As demonstrated in studies of osteonecrosis of the femoral head (35), bone marrow edema distal to the infarct constitutes an indirect sign of articular collapse. The edema spares the devascularized infarcted segment. The fracture of the subchondral bone plate can show two patterns at MRI (19,29): *(a)* depression of the subchondral bone plate with loss of epiphyseal contour or *(b)* more rarely seen in the knee, a high-signal-intensity line on T2-weighted MR images extending under the subchondral bone plate representing fluid accumulating in the subchondral fracture cleft. These two patterns may coexist. As demonstrated in studies (36–38) of osteonecrosis of the femoral head,

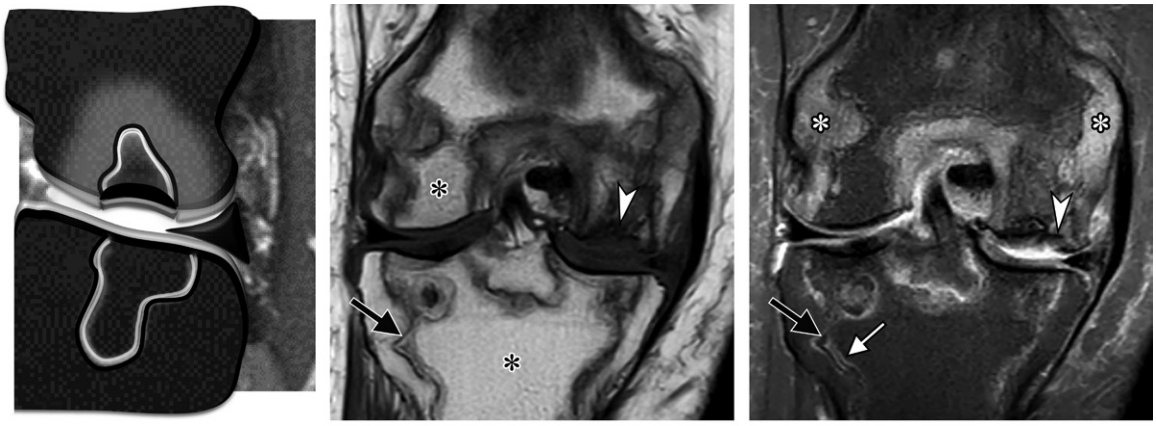

a. b. c.

Figure 11. AVN of the knee in a 59-year-old woman who was undergoing long-term corticosteroid treatment. Diagram of image from a fluid-sensitive sequence **(a)**, coronal T1-weighted MR image **(b)**, and proton-density–weighted fat-suppressed MR image **(c)** show multiple regions of AVN in the femur and tibia. Necrotic areas show preserved fatty marrow signal intensity (∗ in **b**), outlined with sclerosis (black arrow in **b** and **c**) and granulation tissue (white arrow in **c**), producing a double-line sign. Note articular surface collapse of the medial femoral condyle (arrowhead in **b** and **c**), with depression of the subchondral bone plate **(c)** and loss of subchondral fatty signal intensity **(b)**. Bone marrow edema surrounding the infarct is present on the femoral side (∗ in **c**) but not on the tibial side.

radiography and, in particular, CT are superior to MRI in demonstrating subchondral fracture. After articular collapse, the signal in the necrotic segment changes because of fragmentation, invasion of fibrovascular tissue, and secondary cyst formation. Normal fatty signal intensity on T1-weighted images is lost and replaced with inhomogeneous low to intermediate signal intensity (30), most prominently in the weight-bearing area of the infarct (Fig 12).

Juvenile and Adult OCD

OCD is a focal idiopathic alteration of subchondral bone with a risk for instability and disruption of adjacent articular cartilage that may result in premature osteoarthritis (39,40). This condition remains poorly understood and, despite years of collaborative research, there is no consensus regarding its etiology, natural history, or treatment (41,42). The unique feature of this condition is that separation and detachment of the osteochondral fragment culminate the process that originally starts deep underneath the articular surface (43) and subsequently involves the articular cartilage at the peripheral border of the lesion: an "inside-out" mechanism. In comparison, acute traumatic osteochondral injury first affects articular cartilage and then, with sufficient magnitude of force, proceeds to disrupt subchondral bone (2): an "outside-in" mechanism.

A hypothesis that juvenile OCD is produced by a disruption of endochondral ossification of the epiphysis was introduced in early studies (43–45) and was further developed in more recent work on the basis of MRI observations (46) (Fig 13). In summary, an unknown insult causes a disturbance of a small area of the epiphyseal growth plate, which results in localized delay or cessation of normal ossification. The epiphyseal segment in the area of disturbance remains cartilaginous, while the rest of the epiphysis continues to ossify and expand in a centrifugal fashion, creating an appearance of a radiolucent crater that corresponds to the area of hindered cartilage ossification.

This segment, "a progeny," may later develop laminar calcifications in the deep areas or may ossify partially or completely (45). Presumably, when an OCD lesion cannot withstand forces applied to the joint surface, it begins to separate from the "parent" bone. Detachment first starts at the deep, basal portion of the lesion, producing a cleft at the interface (47–49), which leads to fragment instability, with subsequent disruption of the bone plate and overlying articular cartilage and eventual fragment separation.

Histologic core biopsy specimens obtained in juvenile OCD lesions showed that osteonecrosis is either absent (47,50) or infrequent (48,51). Although definitive evidence is lacking, when osteonecrosis is found in OCD, it actually may be secondary to fragment detachment and loss of blood supply rather than the primary cause of its formation (41,43,45,50).

The condition can manifest either in childhood (juvenile OCD) or middle age (adult OCD), but the most frequent age of onset is in preadolescence. Authors of many studies have emphasized the role of chronic repetitive trauma in active children, particularly those who are high-level athletes (52,53). Patients experience poorly localized knee

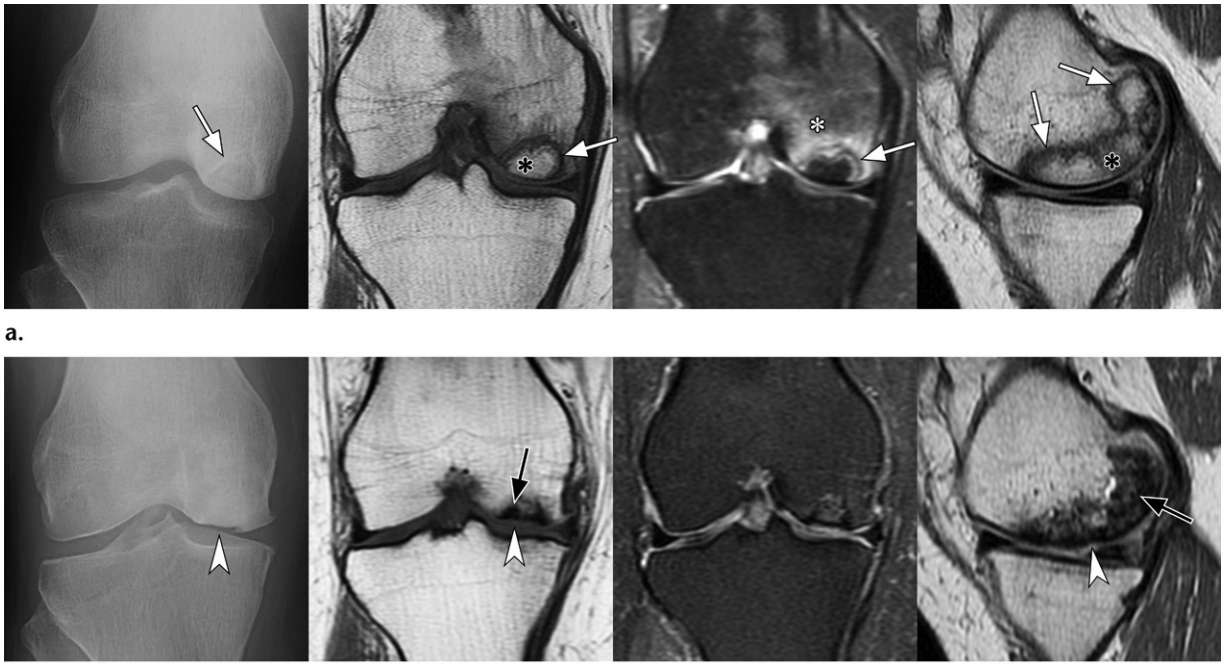

Figure 12. AVN of the medial femoral condyle in a 29-year-old woman with lupus. Radiographs, coronal T1-weighted images, proton-density–weighted fat-suppressed images, and sagittal proton-density–weighted images (left to right in rows **a** and **b**) were obtained at the onset of knee pain **(a)** and 7 years later **(b)**. **(a)** Initially, a large area of necrosis shows normal marrow signal intensity that represents mummified fat (black ∗) outlined with a sclerotic rim (arrows) that is convex to the articular surface. Although the articular surface and subchondral bone plate are intact, the presence of bone marrow edema surrounding the AVN (white ∗) suggests an impending articular collapse. Note the lack of edema in the necrotic segment. **(b)** Subsequently, a frank articular collapse (arrowheads) has developed, followed by loss of fatty signal intensity in the necrotic area (arrows).

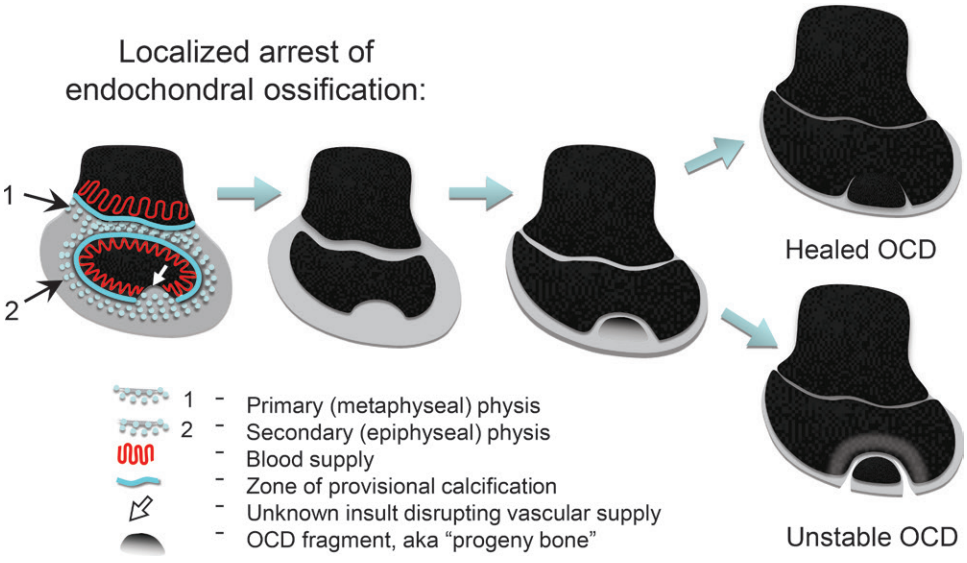

Figure 13. Illustration shows the hypothesized pathogenesis of juvenile OCD as a growth disturbance of the secondary physis that causes a localized delay of ossification and subchondral bone formation, followed by either healing or failure of the overlying cartilage and localized articular surface fragmentation and separation. Based on Barrie and Laor et al (43,46).

pain for more than 1 year before diagnosis, often exacerbated by exercise (41), or with mechanical symptoms caused by dislodging of the fragment.

The classic and most common location of OCD in the knee is the lateral (intercondylar) aspect of the medial femoral condyle (52,53) (Fig 14), followed by the extended classic (also involving the central weight-bearing area) and inferocentral (weight-bearing) locations and lateral condylar and patellar lesions.

The majority of OCD lesions can be diagnosed radiographically; however, there is, to our

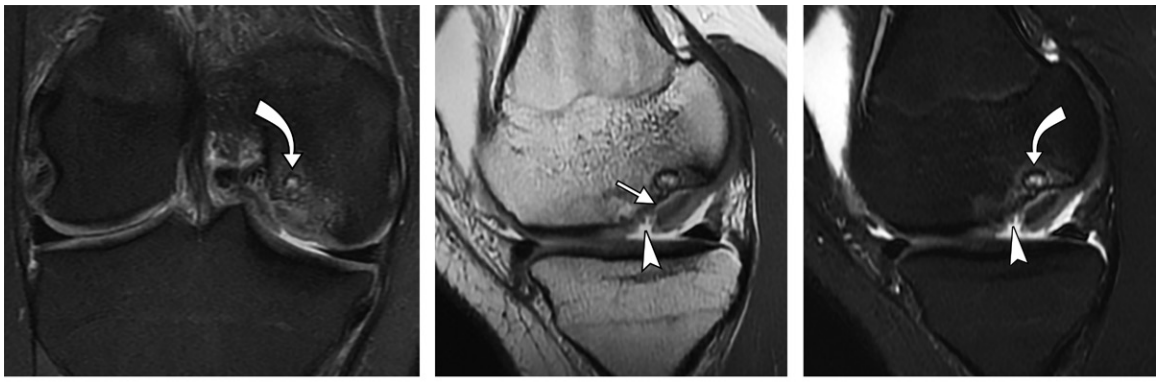

a. b. c.

Figure 14. Unstable OCD lesion in a 17-year-old boy. Coronal proton-density–weighted fat-suppressed MR image **(a)** sagittal proton-density–weighted MR image **(b)**, and T2-weighted fat-suppressed MR image **(c)** show an OCD lesion in a classic location at the lateral aspect of the medial femoral condyle with cysts (curved arrow in **a** and **c**) and a high-signal-intensity rim (straight arrow in **b**) at the interface between the fragment and parent bone associated with breaks in the subchondral bone plate and articular cartilage along the periphery of the lesion (arrowhead in **b** and **c**).

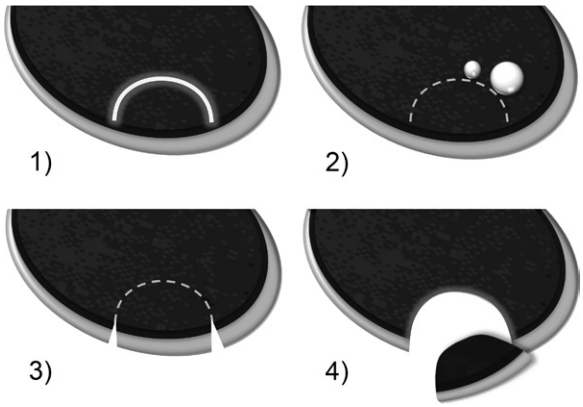

Figure 15. Diagram shows the classic four signs of instability in an OCD lesion: *1,* high signal intensity rim at the interface between the fragment and the adjacent bone on T2-weighted MR images; *2,* fluid-filled cysts beneath the lesion; *3,* a high-signal-intensity line extending through the articular cartilage overlying the lesion; and *4,* a focal osteochondral defect filled with joint fluid. Additional secondary criteria are employed for a juvenile OCD lesion to increase specificity.

knowledge, no current consensus on radiographic features that can be used for assessment of healing or even on a definition of OCD healing in general (41). The multicenter study group Research in OCD of the Knee (ROCK) recently has proposed a radiographic classification system to improve interobserver reliability (54).

MRI can allow characterization of various tissue compositions of the progeny fragment (51,55). Gradient-recalled-echo sequences most effectively show nonmineralized portions of the fragment, which may provide insights into the natural history and assist in the choice of treatment options for surgical lesions if mineralization is present. The absence of bone marrow edema, morphology and location of the lesion, and the age of the patient should aid in the important differentiation of a developmental variant of ossification from OCD (56,57).

Two essential factors allow determination of the prognosis and treatment strategies for OCD: the skeletal maturity of the patient and the stability of the lesion (41,58,59). Skeletal maturity must be determined first, because MRI criteria for instability for adults differ from those for juvenile OCD. The four classic signs of instability described at MRI include (60,61) (Figs 14, 15): *(a)* a high-signal-intensity rim at the interface between the fragment and the adjacent bone on T2-weighted MR images; *(b)* fluid-filled cysts beneath the lesion; *(c)* a high-signal-intensity line extending through the articular cartilage overlying the lesion; and *(d)* a focal osteochondral defect filled with joint fluid, indicating complete detachment of the fragment (Fig 16). The presence of any one sign indicates instability in adult OCD, the most frequent finding being an underlying high-signal-intensity line (61). When all four criteria are met, they have 100% sensitivity and 100% specificity for instability in adult OCD and 100% sensitivity but only 11% specificity for instability in juvenile OCD lesions (62) (Fig 17).

These criteria were revised for juvenile OCD (62) with the addition of three secondary signs that all showed 100% specificity: *(a)* a T2-weighted high-signal-intensity rim surrounding a juvenile OCD lesion indicates instability only if it has the same signal intensity as that of joint fluid, *(b)* a second outer rim of T2-weighted low signal intensity, or *(c)* multiple breaks in the subchondral bone plate on T2-weighted MR images (Fig 18). The rim of fluid signal intensity surrounding an OCD lesion most likely represents a fluid-filled cleft between the progeny and parent bone, while

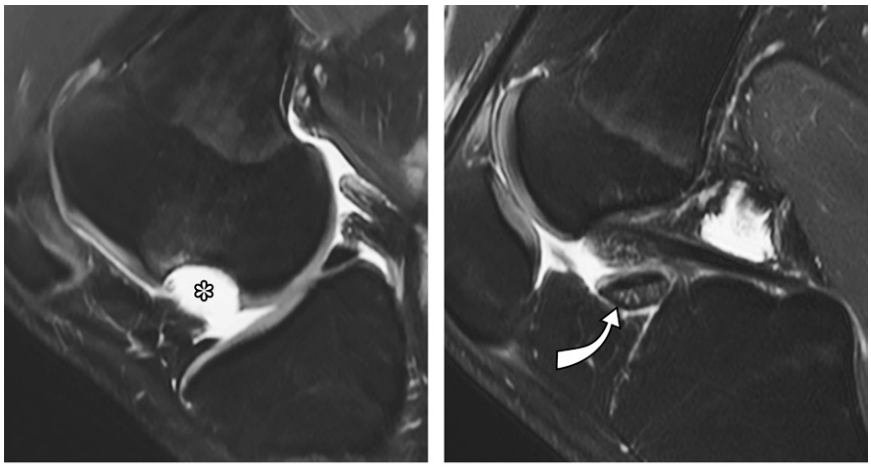

Figure 16. OCD in an 18-year-old man who heard a pop while getting out of bed and was unable to extend his knee. Sagittal T2-weighted fat-suppressed MR images of the knee obtained through the medial compartment **(a)** and the posterior cruciate ligament **(b)** show a large crater at the medial femoral condyle (* in **a**) and an OCD fragment (arrow in **b**) displaced into the intercondylar notch.

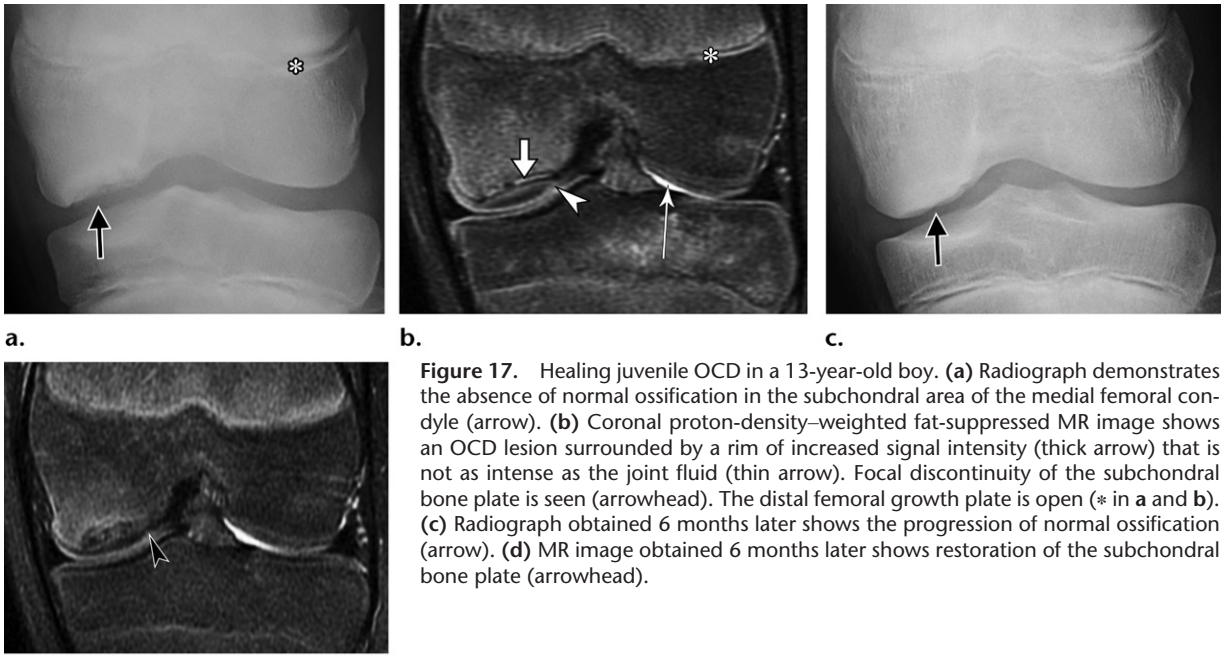

Figure 17. Healing juvenile OCD in a 13-year-old boy. **(a)** Radiograph demonstrates the absence of normal ossification in the subchondral area of the medial femoral condyle (arrow). **(b)** Coronal proton-density–weighted fat-suppressed MR image shows an OCD lesion surrounded by a rim of increased signal intensity (thick arrow) that is not as intense as the joint fluid (thin arrow). Focal discontinuity of the subchondral bone plate is seen (arrowhead). The distal femoral growth plate is open (* in **a** and **b**). **(c)** Radiograph obtained 6 months later shows the progression of normal ossification (arrow). **(d)** MR image obtained 6 months later shows restoration of the subchondral bone plate (arrowhead).

an outer rim of low signal intensity may represent organized fibrous tissue or sclerotic bone at the interface (50,51). When combined, these secondary MRI findings have 100% sensitivity and 100% specificity for detection of unstable juvenile OCD lesions. Cysts surrounding a juvenile OCD lesion indicate instability only if they are multiple or larger than 5 mm (62).

Symptomatic unstable lesions are often treated surgically (42,59), with the choice of technique depending on whether the fragment is salvageable or not (58,59). An unstable fragment may be unsalvageable when it consists of cartilage only (no bone on the deep surface), is composed of multiple pieces, or contains damaged or absent articular cartilage (58). MRI is a valuable diagnostic tool that provides critical information about the composition, stability, and integrity of the OCD fragment. Arthroscopic parameters used to evaluate OCD continue to evolve with the recent classification system introduced by the ROCK study group, which showed excellent intra- and interobserver reliability (63).

Osteochondral Lesions Related to Arthritis

Conditions that affect articular cartilage are frequently accompanied by abnormalities in the subchondral marrow. In osteoarthritis, such abnormalities include bone sclerosis (referred to as *eburnation* on radiographs), bone marrow edema-like lesions, and subchondral cystlike lesions (Fig 19). The suffix "-like" is used because of a large spectrum of histologic changes responsible for these patterns of signal intensity alteration on MR images. *Bone marrow edema-like lesion*, the term adopted by the osteoarthritis

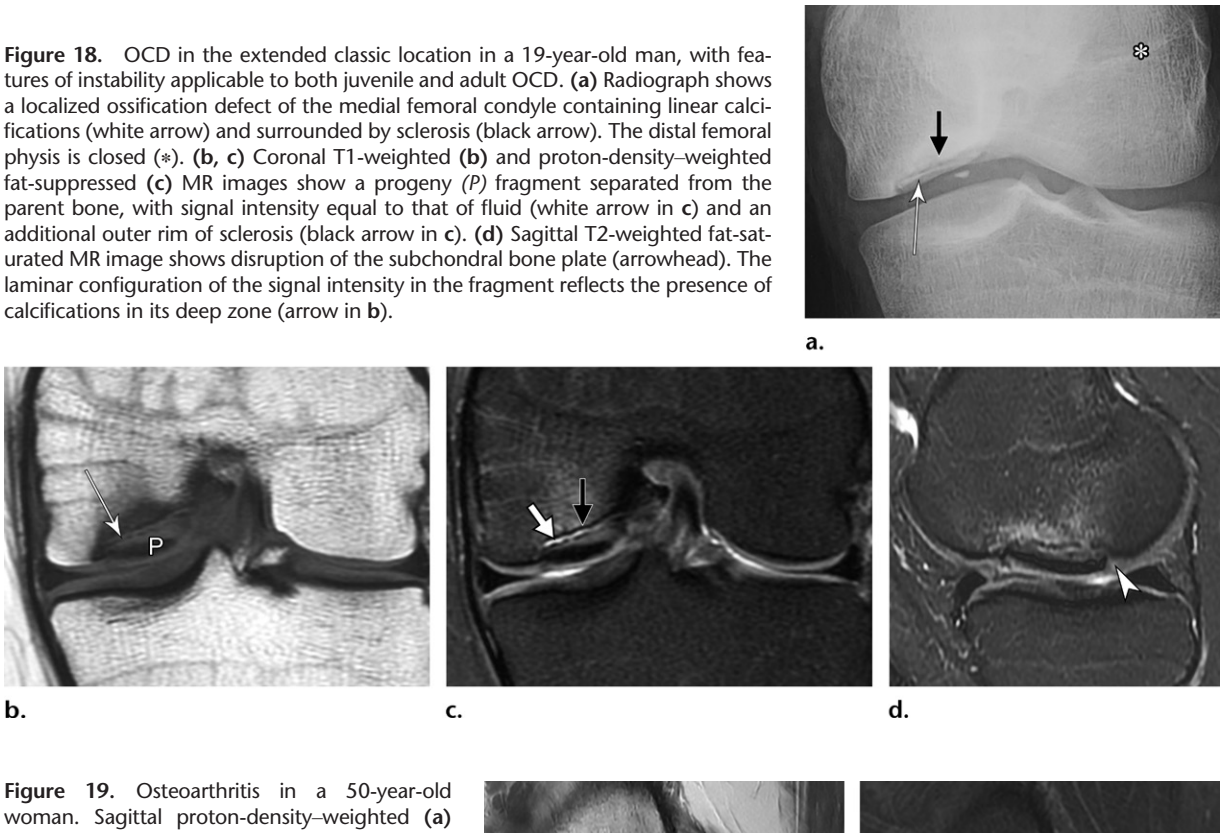

Figure 18. OCD in the extended classic location in a 19-year-old man, with features of instability applicable to both juvenile and adult OCD. **(a)** Radiograph shows a localized ossification defect of the medial femoral condyle containing linear calcifications (white arrow) and surrounded by sclerosis (black arrow). The distal femoral physis is closed (*). **(b, c)** Coronal T1-weighted **(b)** and proton-density–weighted fat-suppressed **(c)** MR images show a progeny *(P)* fragment separated from the parent bone, with signal intensity equal to that of fluid (white arrow in **c**) and an additional outer rim of sclerosis (black arrow in **c**). **(d)** Sagittal T2-weighted fat-saturated MR image shows disruption of the subchondral bone plate (arrowhead). The laminar configuration of the signal intensity in the fragment reflects the presence of calcifications in its deep zone (arrow in **b**).

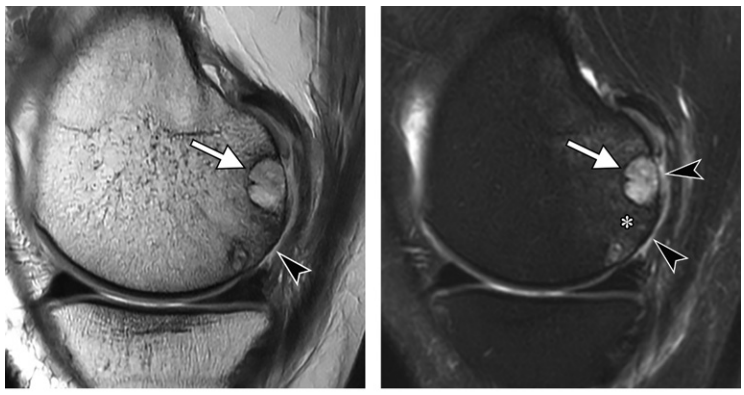

Figure 19. Osteoarthritis in a 50-year-old woman. Sagittal proton-density–weighted **(a)** and T2-weighted fat-suppressed **(b)** MR images of the medial femoral condyle show subchondral cystlike lesions (arrow) and bone marrow edema-like lesions (* in **b**). Full-thickness cartilage loss is present (arrowheads), accompanied by subchondral sclerosis (immediately under the tissue near the arrowhead in **a**).

research community, is defined as a noncystic subchondral area of ill-defined hyperintensity on fluid-sensitive sequences and hypointensity on T1-weighted images.

The most common histologic findings in bone marrow edema-like lesions include bone necrosis, fibrosis, hemorrhage, and trabecular abnormalities, while edema is infrequent (64–66). Subchondral cystlike lesions are well-defined rounded areas of fluid signal intensity; they may contain necrotic bone debris, myxoid and adipose tissue, fibrous elements, or proteinaceous material and are lined by a nonepithelial fibrous wall (67,68).

There are two theories of pathogenesis of subchondral cyst formation: the *synovial fluid intrusion theory*, which proposes that articular surface defects and increased intra-articular pressure allow intrusion of synovial fluid into the bone, leading to formation of cavities; and the *bone contusion theory,* according to which noncommunicating cysts arise from subchondral foci of bone necrosis that are the result of opposing articular surfaces coming in contact with each other (67,69,70). Although there is evidence that both mechanisms may operate together, results of recent studies (71,72) support the bone contusion theory of osteoarthritis by showing that subchondral cysts arise in preexisting regions of subchondral bone marrow edema-like lesions, and their development is predicted much more strongly by bone marrow edema-like lesions than by full-thickness cartilage loss (71,72). Bone marrow edema-like lesions in osteoarthritis are predictors of pain and progression of cartilage damage and subchondral bone attrition (defined

as flattening or depression of the osseous articular surface unrelated to a fracture) (66,73,74). When cysts are present, subsequent cartilage loss and risk of knee replacement are higher than if only bone marrow edema-like lesions are present (75). In addition to osteoarthritis, subchondral cystlike lesions may be prominent in rheumatoid arthritis and calcium pyrophosphate deposition disease (67). Cysts may be seen accompanying AVN and SIF (19).

Subchondral sclerosis in osteoarthritis is related to a deposition of new bone on preexisting trabeculae and to trabecular compression and microfractures with callus formation (76), although associated histologic abnormalities and MRI signal alterations are far more complex (77). Bone sclerosis in osteoarthritis at MRI may resemble the subchondral low-signal-intensity areas seen in SIF. However, the bone marrow edema-like pattern is typically localized in osteoarthritis and extensive in SIF; articular cartilage may be preserved in early SIF, while significant cartilage loss typically accompanies eburnation in osteoarthritis. Once SIF progresses to collapse and articular surface destruction, distinguishing it from primary osteoarthritis at imaging may be impossible, and it is likely to be clinically irrelevant.

Conclusion

When analyzing osteochondral lesions on MR images of the knee, the radiologist must first consider patient demographics, clinical presentation, and history of trauma. Patients may report acute, chronic repetitive, or minimal but distinct traumatic events or no trauma at all. Second, the subchondral bone marrow and subchondral bone plate must be examined and correlated with the radiographic appearance. MRI features that aid in diagnosis include the location and extent of bone marrow edema, the presence of a fracture line, a hypointense area immediately subjacent to a subchondral bone plate, and a subtle or gross deformity of the bone plate. These are essential findings to acknowledge in patients with acute traumatic injuries and SIF. If the lesion consists of a distinct subchondral region demarcated from the surrounding bone, such demarcation should be examined closely for completeness and the presence of a "double-line sign," as seen in AVN, and for findings of instability, which are important for proper evaluation of OCD.

Finally, it is important to assess the integrity of the overlying articular cartilage. Subchondral bone plate collapse, demonstrated by the presence of a frank depression or a fluid-filled cleft, can be seen in advanced stages of both AVN and SIF, indicating irreversibility. Once the diagnosis is established, it is important to report pertinent MRI findings that may guide appropriate treatment of each condition. An osteochondral defect can be created acutely or, more often, develops as a common final pathway of several chronic conditions. When it is accompanied by secondary osteoarthritis, it may be impossible to determine the original cause of epiphyseal deformity, and treatment options may be limited to joint replacement.

References

1. Looze CA, Capo J, Ryan MK, et al. Evaluation and management of osteochondral lesions of the talus. Cartilage 2017;8(1):19–30.
2. Pathria MN, Chung CB, Resnick DL. Acute and stress-related injuries of bone and cartilage: pertinent anatomy, basic biomechanics, and imaging perspective. Radiology 2016;280(1):21–38.
3. Goodwin DW, Zhu H, Dunn JF. In vitro MR imaging of hyaline cartilage: correlation with scanning electron microscopy. AJR Am J Roentgenol 2000;174(2):405–409.
4. Duncan H, Jundt J, Riddle JM, Pitchford W, Christopherson T. The tibial subchondral plate. a scanning electron microscopic study. J Bone Joint Surg Am 1987;69(8):1212–1220.
5. Clark JM, Huber JD. The structure of the human subchondral plate. J Bone Joint Surg Br 1990;72(5):866–873.
6. Winalski CS, Rajiah P. The evolution of articular cartilage imaging and its impact on clinical practice. Skeletal Radiol 2011;40(9):1197–1222.
7. McGibbon CA, Bencardino J, Yeh ED, Palmer WE. Accuracy of cartilage and subchondral bone spatial thickness distribution from MRI. J Magn Reson Imaging 2003;17(6):703–715.
8. Goodwin DW, Wadghiri YZ, Zhu H, Vinton CJ, Smith ED, Dunn JF. Macroscopic structure of articular cartilage of the tibial plateau: influence of a characteristic matrix architecture on MRI appearance. AJR Am J Roentgenol 2004;182(2):311–318.
9. Resnick D. Traumatic disorders of bone. In: Resnick D, Kang HS, Pretterklieber ML, eds. Internal derangements of joints. 2nd ed. Philadelphia, Pa: Saunders/Elsevier, 2006; 259–370.
10. Roemer FW, Frobell R, Hunter DJ, et al. MRI-detected subchondral bone marrow signal alterations of the knee joint: terminology, imaging appearance, relevance and radiological differential diagnosis. Osteoarthritis Cartilage 2009;17(9):1115–1131.
11. Sanders TG, Medynski MA, Feller JF, Lawhorn KW. Bone contusion patterns of the knee at MR imaging: footprint of the mechanism of injury. RadioGraphics 2000;20(Spec No):S135–S151.
12. MacMahon PJ, Palmer WE. A biomechanical approach to MRI of acute knee injuries. AJR Am J Roentgenol 2011;197(3):568–577.
13. Chung CB, Lektrakul N, Resnick D. Straight and rotational instability patterns of the knee: concepts and magnetic resonance imaging. Radiol Clin North Am 2002;40(2):203–216.
14. Ahlbäck S, Bauer GC, Bohne WH. Spontaneous osteonecrosis of the knee. Arthritis Rheum 1968;11(6):705–733.
15. Yamamoto T, Bullough PG. Spontaneous osteonecrosis of the knee: the result of subchondral insufficiency fracture. J Bone Joint Surg Am 2000;82(6):858–866.
16. Takeda M, Higuchi H, Kimura M, Kobayashi Y, Terauchi M, Takagishi K. Spontaneous osteonecrosis of the knee: histopathological differences between early and progressive cases. J Bone Joint Surg Br 2008;90(3):324–329.
17. Lecouvet FE, van de Berg BC, Maldague BE, et al. Early irreversible osteonecrosis versus transient lesions of the femoral condyles: prognostic value of subchondral bone and marrow changes on MR imaging. AJR Am J Roentgenol 1998;170(1):71–77.
18. Ramnath RR, Kattapuram SV. MR appearance of SONK-like subchondral abnormalities in the adult knee: SONK redefined. Skeletal Radiol 2004;33(10):575–581.
19. Lecouvet FE, Malghem J, Maldague BE, Vande Berg BC. MR imaging of epiphyseal lesions of the knee: current

concepts, challenges, and controversies. Radiol Clin North Am 2005;43(4):655–672, vii–viii.
20. Yao L, Stanczak J, Boutin RD. Presumptive subarticular stress reactions of the knee: MRI detection and association with meniscal tear patterns. Skeletal Radiol 2004;33(5):260–264.
21. Plett SK, Hackney LA, Heilmeier U, et al. Femoral condyle insufficiency fractures: associated clinical and morphological findings and impact on outcome. Skeletal Radiol 2015; 44(12):1785–1794.
22. Sonoda K, Yamamoto T, Motomura G, Karasuyama K, Kubo Y, Iwamoto Y. Fat-suppressed T2-weighted MRI appearance of subchondral insufficiency fracture of the femoral head. Skeletal Radiol 2016;45(11):1515–1521.
23. Viana SL, Machado BB, Mendlovitz PS. MRI of subchondral fractures: a review. Skeletal Radiol 2014;43(11): 1515–1527.
24. Jose J, Pasquotti G, Smith MK, Gupta A, Lesniak BP, Kaplan LD. Subchondral insufficiency fractures of the knee: review of imaging findings. Acta Radiol 2015;56(6):714–719.
25. Bedi A, Kelly NH, Baad M, et al. Dynamic contact mechanics of the medial meniscus as a function of radial tear, repair, and partial meniscectomy. J Bone Joint Surg Am 2010;92 (6):1398–1408.
26. Brahme SK, Fox JM, Ferkel RD, Friedman MJ, Flannigan BD, Resnick DL. Osteonecrosis of the knee after arthroscopic surgery: diagnosis with MR imaging. Radiology 1991;178(3):851–853.
27. Jordan RW, Aparajit P, Docker C, Udeshi U, El-Shazly M. The importance of early diagnosis in spontaneous osteonecrosis of the knee: a case series with six year follow-up. Knee 2016;23(4):702–707.
28. Murphey MD, Foreman KL, Klassen-Fischer MK, Fox MG, Chung EM, Kransdorf MJ. Imaging of osteonecrosis: radiologic-pathologic correlation. RadioGraphics 2014;34(4):1003–1028.
29. Vande Berg BC, Lecouvet FE, Maldague B, Malghem J. Osteonecrosis and transient osteoporosis of the femoral head. In: Davies AM, Johnson KJ, Whitehouse RW, eds. Imaging of the hip and bony pelvis. Medical radiology series (diagnostic imaging). Berlin, Germany: Springer, 2006; 195–216.
30. Vande Berg BE, Malghem JJ, Labaisse MA, Noel HM, Maldague BE. MR imaging of avascular necrosis and transient marrow edema of the femoral head. RadioGraphics 1993; 13(3):501–520.
31. Bullough PG, DiCarlo EF. Subchondral avascular necrosis: a common cause of arthritis. Ann Rheum Dis 1990;49(6): 412–420.
32. Karasuyama K, Yamamoto T, Motomura G, Sonoda K, Kubo Y, Iwamoto Y. The role of sclerotic changes in the starting mechanisms of collapse: a histomorphometric and FEM study on the femoral head of osteonecrosis. Bone 2015;81:644–648.
33. Motomura G, Yamamoto T, Yamaguchi R, et al. Morphological analysis of collapsed regions in osteonecrosis of the femoral head. J Bone Joint Surg Br 2011;93(2):184–187.
34. Sakai T, Sugano N, Ohzono K, Matsui M, Hiroshima K, Ochi T. MRI evaluation of steroid- or alcohol-related osteonecrosis of the femoral condyle. Acta Orthop Scand 1998;69(6):598–602.
35. Iida S, Harada Y, Shimizu K, et al. Correlation between bone marrow edema and collapse of the femoral head in steroid-induced osteonecrosis. AJR Am J Roentgenol 2000;174(3):735–743.
36. Stevens K, Tao C, Lee SU, et al. Subchondral fractures in osteonecrosis of the femoral head: comparison of radiography, CT, and MR imaging. AJR Am J Roentgenol 2003;180 (2):363–368.
37. Yeh LR, Chen CK, Huang YL, Pan HB, Yang CF. Diagnostic performance of MR imaging in the assessment of subchondral fractures in avascular necrosis of the femoral head. Skeletal Radiol 2009;38(6):559–564.
38. Hu LB, Huang ZG, Wei HY, Wang W, Ren A, Xu YY. Osteonecrosis of the femoral head: using CT, MRI and gross specimen to characterize the location, shape and size of the lesion. Br J Radiol 2015;88(1046):20140508.
39. Edmonds EW, Shea KG. Osteochondritis dissecans: editorial comment. Clin Orthop Relat Res 2013;471(4): 1105–1106.
40. Carey JL, Shea KG. AAOS appropriate use criteria: management of osteochondritis dissecans of the femoral condyle. J Am Acad Orthop Surg 2016;24(9):e105–e111.
41. Edmonds EW, Polousky J. A review of knowledge in osteochondritis dissecans: 123 years of minimal evolution from König to the ROCK study group. Clin Orthop Relat Res 2013;471(4):1118–1126.
42. Chambers HG, Shea KG, Anderson AF, et al. American Academy of Orthopaedic Surgeons clinical practice guideline on: the diagnosis and treatment of osteochondritis dissecans. J Bone Joint Surg Am 2012;94(14):1322–1324.
43. Barrie HJ. Osteochondritis dissecans 1887-1987: a centennial look at König's memorable phrase. J Bone Joint Surg Br 1987;69(5):693–695.
44. Ribbing S. Studies on hereditary, multiple epiphyseal disorder. Acta Radiol 1937;34:1–107.
45. Barrie HJ. Hypertrophy and laminar calcification of cartilage in loose bodies as probable evidence of an ossification abnormality. J Pathol 1980;132(2):161–168.
46. Laor T, Zbojniewicz AM, Eismann EA, Wall EJ. Juvenile osteochondritis dissecans: is it a growth disturbance of the secondary physis of the epiphysis? AJR Am J Roentgenol 2012;199(5):1121–1128.
47. Yonetani Y, Nakamura N, Natsuume T, Shiozaki Y, Tanaka Y, Horibe S. Histological evaluation of juvenile osteochondritis dissecans of the knee: a case series. Knee Surg Sports Traumatol Arthrosc 2010;18(6):723–730.
48. Uozumi H, Sugita T, Aizawa T, Takahashi A, Ohnuma M, Itoi E. Histologic findings and possible causes of osteochondritis dissecans of the knee. Am J Sports Med 2009;37(10): 2003–2008.
49. Barrie HJ. Hypothesis--a diagram of the form and origin of loose bodies in osteochondritis dissecans. J Rheumatol 1984;11(4):512–513.
50. Krause M, Lehmann D, Amling M, et al. Intact bone vitality and increased accumulation of nonmineralized bone matrix in biopsy specimens of juvenile osteochondritis dissecans: a histological analysis. Am J Sports Med 2015; 43(6):1337–1347.
51. Zbojniewicz AM, Stringer KF, Laor T, Wall EJ. Juvenile osteochondritis dissecans: correlation between histopathology and MRI. AJR Am J Roentgenol 2015;205(1): W114–W123.
52. Aichroth P. Osteochondritis dissecans of the knee: a clinical survey. J Bone Joint Surg Br 1971;53(3):440–447.
53. Hefti F, Beguiristain J, Krauspe R, et al. Osteochondritis dissecans: a multicenter study of the European Pediatric Orthopedic Society. J Pediatr Orthop B 1999;8(4): 231–245.
54. Wall EJ, Polousky JD, Shea KG, et al. Novel radiographic feature classification of knee osteochondritis dissecans: a multicenter reliability study. Am J Sports Med 2015;43(2): 303–309.
55. Ellermann J, Johnson CP, Wang L, Macalena JA, Nelson BJ, LaPrade RF. Insights into the epiphyseal cartilage origin and subsequent osseous manifestation of juvenile osteochondritis dissecans with a modified clinical MR imaging protocol: a pilot study. Radiology 2017;282(3):798–806.
56. Gebarski K, Hernandez RJ. Stage-I osteochondritis dissecans versus normal variants of ossification in the knee in children. Pediatr Radiol 2005;35(9):880–886.
57. Jans LB, Jaremko JL, Ditchfield M, Huysse WC, Verstraete KL. MRI differentiates femoral condylar ossification evolution from osteochondritis dissecans: a new sign. Eur Radiol 2011;21(6):1170–1179.
58. Shea KG, Carey JL, Brown GA, Murray JN, Pezold R, Sevarino KS. Management of osteochondritis dissecans of the femoral condyle. J Am Acad Orthop Surg 2016;24(9): e102–e104.
59. Carey JL, Grimm NL. Treatment algorithm for osteochondritis dissecans of the knee. Orthop Clin North Am 2015;46 (1):141–146.
60. De Smet AA, Fisher DR, Graf BK, Lange RH. Osteochondritis dissecans of the knee: value of MR imaging in deter-

mining lesion stability and the presence of articular cartilage defects. AJR Am J Roentgenol 1990;155(3):549–553.
61. De Smet AA, Ilahi OA, Graf BK. Reassessment of the MR criteria for stability of osteochondritis dissecans in the knee and ankle. Skeletal Radiol 1996;25(2):159–163.
62. Kijowski R, Blankenbaker DG, Shinki K, Fine JP, Graf BK, De Smet AA. Juvenile versus adult osteochondritis dissecans of the knee: appropriate MR imaging criteria for instability. Radiology 2008;248(2):571–578.
63. Carey JL, Wall EJ, Grimm NL, et al. Novel arthroscopic classification of osteochondritis dissecans of the knee: a multicenter reliability study. Am J Sports Med 2016;44(7):1694–1698.
64. Zanetti M, Bruder E, Romero J, Hodler J. Bone marrow edema pattern in osteoarthritic knees: correlation between MR imaging and histologic findings. Radiology 2000;215(3):835–840.
65. Taljanovic MS, Graham AR, Benjamin JB, et al. Bone marrow edema pattern in advanced hip osteoarthritis: quantitative assessment with magnetic resonance imaging and correlation with clinical examination, radiographic findings, and histopathology. Skeletal Radiol 2008;37(5):423–431.
66. Xu L, Hayashi D, Roemer FW, Felson DT, Guermazi A. Magnetic resonance imaging of subchondral bone marrow lesions in association with osteoarthritis. Semin Arthritis Rheum 2012;42(2):105–118.
67. Resnick D, Niwayama G, Coutts RD. Subchondral cysts (geodes) in arthritic disorders: pathologic and radiographic appearance of the hip joint. AJR Am J Roentgenol 1977;128(5):799–806.
68. Pouders C, De Maeseneer M, Van Roy P, Gielen J, Goossens A, Shahabpour M. Prevalence and MRI-anatomic correlation of bone cysts in osteoarthritic knees. AJR Am J Roentgenol 2008;190(1):17–21.
69. Landells JW. The bone cysts of osteoarthritis. J Bone Joint Surg Br 1953;35-B(4):643–649.
70. Rhaney K, Lamb DW. The cysts of osteoarthritis of the hip; a radiological and pathological study. J Bone Joint Surg Br 1955;37-B(4):663–675.
71. Carrino JA, Blum J, Parellada JA, Schweitzer ME, Morrison WB. MRI of bone marrow edema-like signal in the pathogenesis of subchondral cysts. Osteoarthritis Cartilage 2006;14(10):1081–1085.
72. Crema MD, Roemer FW, Zhu Y, et al. Subchondral cyst-like lesions develop longitudinally in areas of bone marrow edema-like lesions in patients with or at risk for knee osteoarthritis: detection with MR imaging—the MOST study. Radiology 2010;256(3):855–862.
73. Roemer FW, Guermazi A, Javaid MK, et al. Change in MRI-detected subchondral bone marrow lesions is associated with cartilage loss: the MOST study: a longitudinal multicentre study of knee osteoarthritis. Ann Rheum Dis 2009;68(9):1461–1465.
74. Roemer FW, Neogi T, Nevitt MC, et al. Subchondral bone marrow lesions are highly associated with, and predict subchondral bone attrition longitudinally: the MOST study. Osteoarthritis Cartilage 2010;18(1):47–53.
75. Tanamas SK, Wluka AE, Pelletier JP, et al. The association between subchondral bone cysts and tibial cartilage volume and risk of joint replacement in people with knee osteoarthritis: a longitudinal study. Arthritis Res Ther 2010;12(2): R58.
76. Gupta KB, Duryea J, Weissman BN. Radiographic evaluation of osteoarthritis. Radiol Clin North Am 2004;42(1):11–41, v.
77. Bergman AG, Willén HK, Lindstrand AL, Pettersson HT. Osteoarthritis of the knee: correlation of subchondral MR signal abnormalities with histopathologic and radiographic features. Skeletal Radiol 1994;23(6):445–448.